Unexpectedly high concentrations of atmospheric mercury species in Lhasa, the largest city on the Tibetan Plateau

Huiming Lin[1], Yindong Tong[2,3]*, Long Chen[4], Chenghao Yu[5], Zhaohan Chu[1], Qianru Zhang[1], Xiufeng Yin[6], Qianggong Zhang[7,8], Shichang Kang[6,8], Junfeng Liu[1], James Schauer[9,10], Benjamin de Foy[11], Xuejun Wang[1]**

1. MOE Laboratory of Earth Surface Processes, College of Urban and Environmental Sciences, Peking University, Beijing 100871, China;

2. School of Science, Tibet University, Lhasa 850000, China

3. School of Environmental Science and Engineering, Tianjin University, Tianjin, 300072, China;

4. School of Geographic Sciences, East China Normal University, Shanghai 200241, China;

5. Key Laboratory of Microbial Technology for Industrial Pollution Control of Zhejiang Province, College of Environment, Zhejiang University of Technology, Hangzhou 310014, China

6. State Key Laboratory of Cryospheric Science, Northwest Institute of Eco-Environment and Resources, Chinese Academy of Sciences, Lanzhou 730000, China

7. Key Laboratory of Tibetan Environment Changes and Land Surface Processes, Institute of Tibetan Plateau Research, Chinese Academy of Sciences, Beijing, 100101, China;

8. CAS Center for Excellence in Tibetan Plateau Earth Sciences, Beijing, 100085, China;

9. Department of Civil and Environmental Engineering, University of Wisconsin-Madison, Madison, WI, USA;

10. Wisconsin State Laboratory of Hygiene, University of Wisconsin-Madison, WI, USA;

11. Department of Earth and Atmospheric Sciences, Saint Louis University, St. Louis, MO, 63108, USA

Correspondence:

*Xuejun Wang (wangxuejun@pku.edu.cn) **Yindong Tong (yindongtong@tju.edu.cn)

Abstract

Lhasa City is located in the central Tibetan Plateau and is the most densely populated area. As the first continuous monitoring of atmospheric mercury (Hg) species in a city on the Tibetan Plateau, our monitoring in Lhasa showed that the concentrations of gaseous elemental Hg (GEM), gaseous oxidized Hg (GOM), and particle-bound Hg (PBM) during subsequent of the Indian Summer Monsoon (S-ISM) period were 2.73 ± 1.48 ng m^{-3}, 38.4 ± 62.7 pg m^{-3}, and 59.1 ± 181.0 pg m^{-3}, respectively. During the Westerly Circulation (WEC) period, the GEM, GOM and PBM concentrations were 2.11 ± 2.09 ng m^{-3}, 35.8 ± 43.3 pg m^{-3}, and 52.9 ± 90.1 pg m^{-3}, respectively. The GOM and PBM concentrations were higher than those of previous monitoring on the Tibetan Plateau and other provincial capitals in China. Typical high-value occurrence processes were studied to investigate random events with high atmospheric Hg concentrations in Lhasa. Combustion event

nearby or further away may be the main contributor of the high-concentration events. The lowest GEM concentrations occurred in the afternoon and persistently high concentrations were observed at night. The changes in GEM concentrations were consistent with the trends of other pollutant concentrations and contradictory to those of the wind speed. The high GEM concentrations at night can be attributed to the lower boundary layer height and lower wind speed. For both GOM and PBM, higher GOM concentrations occurred during the day and PBM during the night. The results of the principal component analysis indicated that local sources and wind speed are important factors influencing atmospheric Hg concentrations in Lhasa. The trajectory simulation showed that the source of the GEM in Lhasa gradually shifted from the south to the west of Lhasa from the S-ISM to the WEC periods, while both the southern and western sources were important in the late WEC period. The concentrations and change patterns of Hg species in Lhasa were significantly different than those at other monitoring sites on the Tibetan Plateau. Monitoring Hg species in Lhasa shows the possible maximum anthropogenic influences on the Tibetan Plateau and demonstrates the dramatic effect of wind on changes in urban atmospheric Hg concentrations.

1. Introduction

Mercury (Hg) has received worldwide attention owing to its high toxicity and bioaccumulation. Atmospheric mercury (Hg) exists in three different forms: atmospheric gaseous elemental Hg (GEM), gaseous oxidized Hg (GOM), and particle-bound Hg (PBM) (Selin, 2009). They exhibit different behaviors in the environment owing to their various chemical properties (Selin, 2009; Travnikov et al., 2017; Lindberg and Stratton, 1998; Seigneur et al., 2006). Many established monitoring networks for atmospheric Hg exist in North America and Europe (Stylo et al., 2016) including the Atmospheric Mercury Network (AMNet; Gay et al., 2013), the Global Mercury Observation System (GMOS; Sprovieri et al., 2013;Sprovieri et al., 2016), the Canadian Atmospheric Mercury Network (CAMNet; Kellerhals et al., 2003), and the Arctic Monitoring Assessment Programme (AMAP; https://mercury.amap.no/) (Gay et al., 2013; Sprovieri et al., 2013; Sprovieri et al., 2016; Kellerhals et al., 2003). They have been operating for decades and have provided a large amount of atmospheric Hg data. Compared to Europe and the United States, independent research teams have conducted monitoring work in China based on different research

65   interests (Fu et al., 2012a; Fu et al., 2008; Fu et al., 2016; Fu et al., 2019; Liu et al., 2011; Feng et

66   al., 2013; Wang et al., 2015; Hu et al., 2014; Ci et al., 2011; Duan et al., 2017; Liu et al., 2002; Yin

67   et al., 2018; Yin et al., 2020; Lin et al., 2022; Lin et al., 2019). Most monitoring stations are set up

68   only in developed regions, such as eastern and central China, owing to operational difficulties in

69   remote areas. Few studies on atmospheric Hg in western China have been reported; thus, little is

70   known about the overall level of atmospheric Hg in western China. To better employ the Minamata

71   Convention and verify the effect of the implementation of the Convention, monitoring atmospheric

72   Hg concentrations around the globe is significant and can aid in identifying the global Hg transport

73   pattern.

74   The Tibetan Plateau is in the mid-latitudes of the Northern Hemisphere (in central Asia) and is

75   an important area for studying the global Hg circulation. Owing to the high altitude and rough living

76   conditions, there is little Hg research on the Tibetan Plateau. This area is less developed and there

77   are few industrial activities; therefore, it is generally considered a clean region and can be treated

78   as a background condition. However, there are large tourist cities in this area, such as Lhasa, where

79   the number of tourists reached 40,121,522 in 2019 (Tibet Bureau of Statistics, 2020). Local cement

80   production in Tibet reached 10.81 million tons in 2019 (Tibet Bureau of Statistics, 2020).

81   Meanwhile, although the high altitude makes the Tibetan region a natural barrier between inland

82   China and the Indian subcontinent (Qiu, 2008; Yao et al., 2012; Pant et al., 2018), the Tibetan Plateau

83   is potentially influenced by the Indian summer monsoon (ISM) and the Westerly circulation (WEC).

84   Trans-boundary inputs of atmospheric pollutants to the Tibetan Plateau have been demonstrated in

85   pollutant studies such as with persistent organic pollutants and black carbon (Yang et al., 2018; Li

86   et al., 2016b; Zhang et al., 2015b; Pokhrel et al., 2016; Wang et al., 2018; Feng et al., 2019; Zhu et

87   al., 2019). Our previous study on atmospheric Hg in the Qomolangma region (QNNP) also

88   suggested that atmospheric Hg from India can be transported and affect atmospheric Hg

89   concentrations on the Tibetan Plateau as a result of the Indian monsoon (Lin et al., 2019). Hence, it

90   remains unclear whether the Tibetan Plateau can be treated as a background area for studying

91   atmospheric Hg, and further monitoring data are required. Monitoring in the largest cities on the

92   Tibetan Plateau will provide important information and corroboration to address this query.

93   In previous study, Yin et al. (2018) reported GEM concentration data for the Namco region on

94   the Tibetan Plateau from 2012-2014 and found that the GEM concentration at Namco was 1.33 ±

95   0.24 ng m^{-3}, which is lower than the mean GEM concentration in the Northern Hemisphere

96   (Lindberg et al., 2007; Slemr et al., 2015; Venter et al., 2015; Sprovieri et al., 2016; Lan et al., 2012).

97   Our previous study at QNNP (Lin et al., 2019) showed that the atmospheric Hg concentrations were

98   1.42 ± 0.37 ng m^{-3}, 21.4 ± 13.4 pg m^{-3}, and 25.6 ± 19.1 pg m^{-3} for GEM, GOM, and PBM,

99   respectively, close similar to the average GEM concentrations in the Northern Hemisphere

100 (Lindberg et al., 2007; Slemr et al., 2015; Venter et al., 2015; Sprovieri et al., 2016; Lan et al., 2012).

101 The concentrations of atmospheric Hg species in Nyingchi, in the southeast Tibetan Plateau, were

102 very low (1.01±0.27 ng m^{-3}, 12.8±13.3 pg m^{-3}, and 9.3±5.9 pg m^{-3} for GEM, GOM, and PBM,

103 respectively), which may be affected by heavy wet deposition and the large amounts of vegetation

104 in the Yarlung Zangbu/Brahmaputra Grand Canyon (Lin et al., 2022). However, Namco, QNNP

105 and Nyingchi are remote areas on the Plateau, with few populations and industries. During previous

106 studies in Lhasa, the largest city on the Plateau, only dry and wet depositions of atmospheric Hg

107 were analyzed. Monitoring of atmospheric Hg particulate matter (Huang et al., 2016a) indicated that

108 Lhasa has mean particulate Hg levels as high as 224 pg m^{-3} (ranging from 61.2 to 831 pg m^{-3}),

109 which is much higher than expected. Huang et al. (2013) measured the wet deposition of

110 atmospheric Hg in Lhasa in 2010 and showed that the wet depositions of total Hg concentration and

111 particulate Hg concentration were higher during the non-monsoon period than that during the

112 monsoon period. The active Hg was higher during the monsoon than during the non-monsoon period,

113 and they concluded that the wet deposition of Hg originated mainly from local sources. This

114 indicates that atmospheric Hg concentrations in Lhasa may be elevated and further detailed

115 monitoring is needed.

116   In this study, we conducted a high-time-precision atmospheric Hg species monitoring system

117 in Lhasa. We performed continuous measurements of GEM, GOM, and PBM concentrations from

118 subsequent of the Indian Summer Monsoon (S-ISM) period to the WEC period from 2016 to 2017.

119 Based on literature research, this is the first continuous monitoring of atmospheric Hg species in a

120 city on the Tibetan Plateau, and the influence of human activities, meteorological factors, and long-

121 range transportation of pollutants on the diurnal variation of atmospheric Hg in Lhasa is discussed.

122 We combined monitoring with other pollutant concentrations to explore the main factors influencing

123   the local atmospheric Hg concentrations. To determine the detailed source profile of atmospheric

124   Hg, we combined real-time Hg monitoring data with backward trajectory and cluster analyses. This

125   study can help understand atmospheric Hg characteristics in the city of the Plateau and provide

126   scientific support for managerial decision-making.

127   **2.   Material and methods**

128   **2.1   Atmospheric Hg monitoring sites**

129   The monitoring site for atmospheric Hg species in Lhasa was set up on the top floor of the

130   Lhasa station office building in the Institute of Tibetan Plateau Research, Chinese Academy of

131   Sciences, in western Lhasa City (29.64°N, 91.03°E, 3650 m above sea level; Figure 1, Figure S1).

132   The monitoring in Lhasa included the subsequent Indian Summer Monsoon (S-ISM, August 29 to

133   September 30, 2016) and Westerly Circulation (WEC, October 1, 2016 to February 2, 2017) periods

134   from August 29, 2016 to February 2, 2017. To better understand the changes of atmospheric Hg

135   concentrations in different periods, the WEC period was further divided into WEC1 (October 1 to

136   December 30, 2016) and WEC2 (January 1 to February 2, 2017) periods. Lhasa is located in the

137   central region and is the largest city on the Tibetan Plateau, covering an area of approximately 60

138   km^2. The Lhasa population in 2019 was 720,700, accounting for approximately 20.6% of the total

139   population of the Tibet Autonomous Region (Tibet Bureau of Statistics, 2020). The entire city is in

140   a flat river valley surrounded by mountains up to 5,500 m above sea level. During the ISM period

141   (from May to September), the low pressure on the Tibetan Plateau attracts the summer monsoon

142   from the Indian Ocean to the Plateau, exhibiting a wetter monsoon season (Qiu, 2008). During the

143   non-monsoon season (from October to April), the large-scale atmospheric circulation on the Tibetan

144   Plateau is mainly under the control of westerly winds, which largely come from the inland areas of

145   Central Asia, presenting a drier season in Lhasa during this time (Huang et al., 2010; Guo et al.,

146   2015). According to previous studies, the air quality in Lhasa may be influenced by local emissions

147   from anthropogenic activities (e.g., power plants, cement facilities, vehicular traffic, and religious

148   activities) (Li et al., 2008; Cong et al., 2011; Huang et al., 2010; Guo et al., 2015; Wang et al., 2016;

149   Li et al., 2016a) and long-range transboundary atmospheric transport (Huang et al., 2016b; Huang

150   et al., 2016a).

151
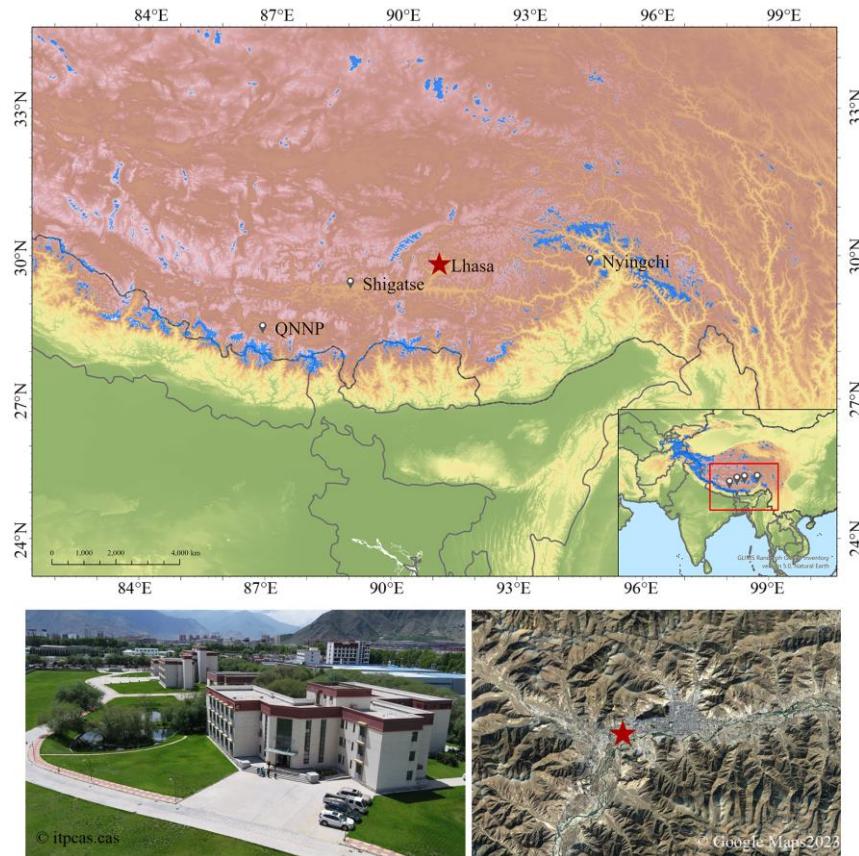
Figure 1 Location of the Lhasa station in the Institute of Tibetan Plateau Research, Chinese Academy of Sciences (red star).

154

2.2 GEM, GOM, and PBM active monitoring

Monitoring in Lhasa was performed using Tekran models 2537 B, 1130, and 1135 (Tekran Inc., Toronto, Canada) for real-time continuous measurements of GEM, GOM, and PBM concentrations. Model 2357b is the main analytical module used to analyze Hg concentrations employing the cold atomic fluorescence technique. Model 1130 is divided into pump and lysimeter modules, which is mainly used for the collection and resolution of GOM. Model 1135 is the particle collection module that is mainly used to collect and analyze atmospheric Hg in the particulate state. During the actual monitoring, considering the low air pressure on the Tibetan Plateau, we reduced the airflow of the pump module to 7.5 L/min (Swartzendruber et al., 2009; Zhang et al., 2015a; Zhang et al., 2016; Lin et al., 2019; Lin et al., 2022) and the airflow in model 2537B was reduced to 1 L/min to ensure that atmospheric Hg monitoring could be continuously performed. All monitoring data were converted to concentrations under standard atmospheric pressure. The Tekran 2537B analyzer was

167 automatically calibrated every 23 hours using the instrument's internal Hg permeation source and

168 was calibrated before and after monitoring using an external Hg source. The same instrument setup

169 was used for QNNP and Nyingchi (Lin et al., 2019; Lin et al., 2022). The Tekran ambient Hg

170 analyzer has been described in detail in previous studies (Landis et al., 2002; Rutter et al. 2008; de

171 Foy et al. 2016).

172 ### 2.3 Meteorological data and other pollutant data

173 During the monitoring period, the Vantage Pro2 weather station (Davis Instruments, USA)

174 recorded local temperature (accuracy of 0.1°C), relative humidity (accuracy of 1%), wind speed

175 (accuracy of 0.1 m s^{-1}), wind direction (accuracy of 1°), barometric pressure (accuracy of 0.1 hPa),

176 solar radiation (accuracy of 1 W m^{-2}), and UV index (accuracy 0.1 MEDs). Hourly measurements

177 of $PM_{2.5}$, PM_{10}, SO_2, NO_2, O_3, and CO concentrations and the air quality index (AQI) were obtained

178 from monitoring stations hosted by the Ministry of Ecology and Environment of China and

179 published by the China Environmental Monitoring Center. The station was set up 10 km from the

180 atmospheric Hg monitoring station.

181 ### 2.4 Backward trajectory simulation and potential source analysis

182 To better understand the transport paths of atmospheric GEM, the Hybrid Single-Particle

183 Lagrangian Integrated Trajectory (HYSPLIT) model was used to calculate backward trajectories

184 (Stein et al., 2015; Chai et al., 2017; Chai et al., 2016; Hurst and Davis, 2017; Lin et al., 2019). The

185 HYSPLIT model (https://www.arl.noaa.gov/hysplit/hysplit/) is a hybrid approach that combines

186 Lagrangian and Eulerian methods, which was developed by the National Oceanic and Atmospheric

187 Administration (NOAA) as a tool to explain the transport, dispersion, and deposition of particles in

188 the atmosphere. The backward trajectory simulation used Global Data Assimilation System (GDAS)

189 data with 1°x1° latitude and longitude horizontal spatial resolution and 23 vertical heights every 6

190 hours in this study. We examined the effect of arrival height on the trajectories using different arrival

191 heights (50 m, 100 m, 400 m, and 1,000 m) in December 2016 (Figure S2). The results showed that

192 the calculated trajectories of the air masses were almost the same when the arrival height was below

193 400 m. The trajectory arrival altitude was then set to 100 m a.g.l in this study. The trajectories were

194 computed every 6 hours with an inverse time of 120 hours. The trajectories could cover China,

195 Nepal, India, Pakistan, and most of West Asia. Here, we combined the backward trajectory with

196   real-time Hg monitoring concentrations to represent the trajectories of GEM concentrations. Cluster

197   analysis was performed after the trajectory calculation. Cluster analysis can indicate the main

198   trajectory of incoming pathways and the GEM concentration indicated by the incoming trajectories.

199   **2.5 Principal component analysis**

200   Principal component analysis (PCA) is a data reduction method that allows a number of

201   measured variables to be categorized into several factors that represent the behavior of the entire

202   dataset (Jackson, 2005). In many previous Hg studies, PCA has been used to analyze the

203   relationships between Hg and multiple pollutants and meteorological variables (Brooks et al., 2010;

204   Cheng et al., 2012; Liu et al., 2007; Zhou et al., 2019; Lin et al., 2022). Prior to running the PCA,

205   all variables were normalized by the standard deviation. To check whether PCA was the appropriate

206   method for the dataset used in this study, Kaiser-Meyer-Olkin's measure of sampling adequacy

207   (MSA>0.5) and Bartlett's Test of sphericity (P<0.05) tests were performed during data analysis.

208   Total variance and rotated scree plots were used to determine the number of factors during the PCA

209   analysis, and components with variance ≥ 1.0 were retained. Variables with high factor loadings

210   (generally >0.5) were identified as potential sources of Hg in this study.

211   **3.   Results and Discussion**

212   **3.1   Atmospheric Hg Monitoring in Lhasa**

213   Atmospheric Hg monitoring in Lhasa comprised the subsequent Indian Summer Monsoon (S-

214   ISM) and Westerly circulation (WEC) periods from August 29, 2016 to February 2, 2017. Figure 2

215   shows the variation in atmospheric Hg concentrations at the station during the monitoring period.

216   During the whole monitoring period, the mean concentrations of GEM, GOM, and PBM at the

217   station were 2.26 ± 1.97 ng m^{-3}, 36.4 ± 48.9 pg m^{-3}, and 54.5 ± 119.5 pg m^{-3} (mean concentration $\pm$

218   standard deviation), respectively. During the S-ISM period, the concentrations of GEM, GOM, and

219   PBM were 2.73 ± 1.48 ng m^{-3}, 38.4 ± 62.7 pg m^{-3}, and 59.1 ± 181.0 pg m^{-3}, respectively. While during

220   the WEC period, the concentrations of GEM, GOM, and PBM were 2.11 ± 2.09 ng m^{-3}, 35.8 ± 43.3

221   pg m^{-3}, and 52.9 ± 90.1 pg m^{-3}, respectively. The GEM concentrations during the S-ISM period were

222   significantly higher than those during the WEC period (p < 0.01), while the mean concentrations of

223   GOM and PBM in the S-ISM period were slightly higher than those in the WEC period. Overall,

224   GEM concentrations showed a decreasing trend throughout the monitoring period, with the average

weekly concentration decreasing from 3.21 ng m^{-3} at the beginning of the monitoring period to 1.60

ng m^{-3} at the end of the monitoring period, which is contrast to previous studies, which showed that

atmospheric Hg concentrations in the Northern Hemisphere is low in summer and high in winter

(Horowitz et al., 2017; Jiskra et al., 2018). The different variation trends between Lhasa and the

whole Northern Hemisphere may be related to the special location of Lhasa. Unexpectedly high

concentrations were found at irregular intervals for all Hg species. The occurrence time of these

high concentrations was random, and high GEM concentrations did not always occur at the same

time as high GOM or PBM concentrations, indicating the complexity of the Hg sources of the

species. For GOM and PBM, relatively comparable trends between them may be related to similar

sources, transport, and transformation reactions in the atmosphere.
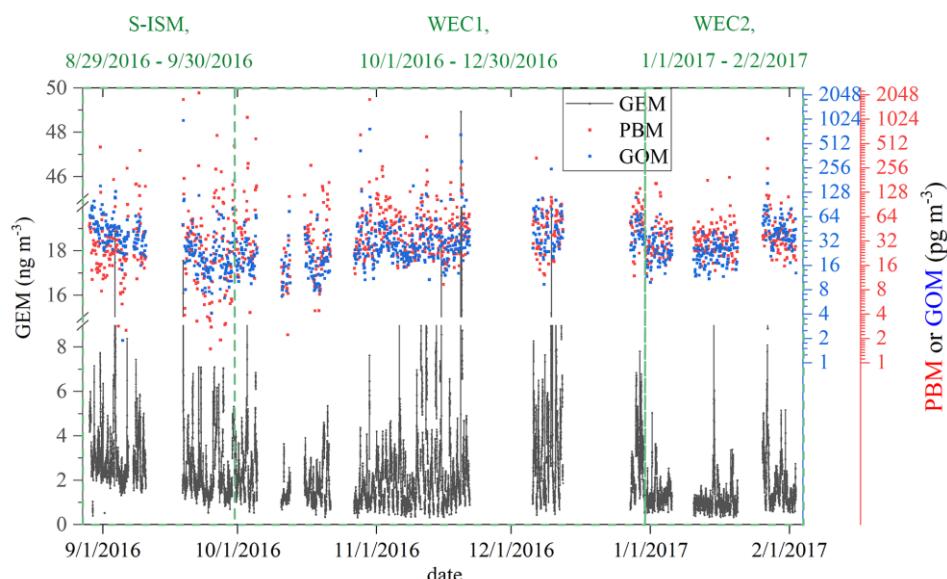
Figure 2 Time series of GEM, GOM, and PBM concentrations over the sampling period. The

GEM concentration resolution was 5 min and the GOM and PBM resolutions was 2 h.

In early September, GOM concentrations were generally higher than PBM concentrations. In

the subsequent period, PBM concentrations were always higher than GOM concentrations, which

may indicate that the sources and composition of pollutants at this time were not consistent with

those in the latter period. GOM and PBM may undergo mutual transformation in the atmosphere,

which may be related to temperature, humidity, and atmospheric composition(Rutter and Schauer,

2007; Rutter et al., 2008), and thus the concentration distributions of GOM and PBM may also be

245   related to the changes of local climate and atmospheric composition from S-ISM to WEC periods.

246   The GOM and PBM concentrations were higher in November and December. Since GOM and PBM

247   are mainly from local emissions, the changes in their concentrations may indicate that there are

248   more local sources at this period. As Lhasa enters the heating season in November-December, and

249   there are more local religious activities at this time, there may be more local combustion sources.

250   Table 1 lists the concentrations of Hg and other pollutants during the monitoring period. $PM_{2.5}$

251   concentration increased significantly in the WEC1 period, indicating the presence of more

252   particulate matter during this period. This could explain the elevated concentrations of GOM and

253   PBM from November-December.

Table 1 Statistics metrics of species Hg, meteorological factors, and other pollutants

Period	Stat	GEM (ng m⁻³)	PBM (pg m⁻³)	GOM (pg m⁻³)	Temp (°C)	Hum. (%)	Wind speed (m s⁻¹)	Solar radiation (W m⁻²)	CO (mg m⁻³)	NO₂ (µg m⁻³)	O₃ (µg m⁻³)	PM₂.₅ (µg m⁻³)	SO₂ (µg m⁻³)
S-ISM	Mean	2.73	59.08	38.39	14.42	61.45	1.70	212.60	0.39	26.44	72.18	16.26	4.19
	SD	1.48	181.38	62.85	3.70	16.96	1.41	313.90	0.18	19.36	28.68	13.12	2.08
	Median	2.36	24.50	30.30	13.90	62.00	1.30	7.00	0.30	22.00	77.00	13.00	4.00
	Min	0.40	-11.44	1.89	5.90	14.00	0.00	0.00	0.10	1.00	1.00	1.00	1.00
	Max	18.87	2165.70	988.50	24.70	93.00	13.00	1290.00	1.70	110.00	133.00	81.00	21.00
WEC1	Mean	2.39	57.55	37.46	6.90	26.01	1.28	169.56	0.64	45.24	45.39	47.97	5.51
	SD	2.35	104.15	50.98	5.75	15.08	1.39	246.66	0.51	31.01	34.44	46.19	5.35
	Median	1.79	38.80	27.83	6.90	24.00	0.90	0.00	0.50	41.00	43.00	35.00	5.00
	Min	0.31	0.00	1.89	-6.20	1.00	0.00	0.00	0.10	2.00	1.00	1.00	1.00
	Max	48.93	1797.30	774.86	21.60	94.00	9.80	973.00	4.40	152.00	133.00	458.00	145.00
WEC2	Mean	1.47	42.82	32.05	0.22	25.59	1.97	123.61	0.56	26.78	65.22	23.73	4.49
	SD	1.12	45.39	17.14	3.98	14.67	1.85	186.98	0.30	22.61	26.30	18.77	2.61
	Median	1.17	33.77	27.50	0.20	24.00	1.30	0.00	0.50	19.00	71.00	19.00	4.00
	Min	0.33	0.00	9.91	-8.80	2.00	0.00	0.00	0.20	2.00	1.00	1.00	1.00
	Max	20.86	589.43	165.06	10.20	68.00	11.20	662.00	2.60	99.00	108.00	118.00	32.00

Table 2 shows the distributions of atmospheric Hg concentrations in some provincial capitals in China and nearby monitoring stations from literature. In general, the GEM concentration in Lhasa is low among the provincial capitals in China. The GEM concentration in other provincial capitals of China was approximately 3-10 ng m⁻³. Guiyang, Chongqing, and Lanzhou were the nearest provincial capitals to Lhasa, with GEM concentrations reported in the literature, all located in

western China. Guiyang had a very high GEM concentration due to the presence of local Hg mines

(Liu et al., 2011). The GEM concentration in Chongqing was approximately three times higher than

that of Lhasa. The higher GEM concentration in Chongqing was likely due to its proximity to the

Hg-contaminated area and large population (Yang et al., 2009). Compared to Lanzhou, another high-

altitude city, the GEM concentration in Lhasa was approximately half that of Lanzhou, which may

be owing to the overall cleaner environment with fewer local pollution sources in Lhasa (Yin et al.,

2020). The GOM and PBM concentrations in other provincial capitals were relatively less monitored.

However, GOM concentrations in Lhasa were significantly higher than those in cities with GOM

monitoring, such as mega-cities like Beijing and Shanghai, and even higher than those in Guiyang,

where Hg mines are located. GOM concentrations in provincial capitals nationwide were mainly

concentrated between 3-20 pg m^{-3}, whereas the GOM concentrations in Lhasa were approximately

2-10 times higher than the average concentration in provincial capitals. The high GOM

concentration in Lhasa is likely due to its high altitude. Lhasa is exposed to much higher solar

radiation and has more ice surfaces than inland areas, which may have contributed to the oxidation

of GEM or the re-release of GOM deposited in snow and ice (Steffen et al., 2008; Dommergue et

al., 2003; Song et al., 2018). In contrast, the PBM concentration in Lhasa was at a lower level, only

somewhat higher than that in Hefei. The monitoring period in Lhasa was mainly in winter when

there were more particulate matter emissions than in summer owing to heating combustion. The

PM$_{2.5}$ concentration in Lhasa was low throughout the monitoring period (Table 1), which indicated

that the local particulate matter emissions were low; this may be the main reason for the low PBM

concentration.

Table 2 Comparison of atmospheric Hg concentrations at some provincial capitals in China and some nearby monitoring stations

location	altitude	type	region	Monitoring period	GEM (ng m⁻³)	GOM (pg m⁻³)	PBM (pg m⁻³)	GEM diurnal variation (local time/GEM concentration)			reference
					$(ng\ m^{-3})$	$(pg\ m^{-3})$	$(pg\ m^{-3})$	Peak $(ng\ m^{-3})$	Valley $(ng\ m^{-3})$	Variation $(ng\ m^{-3})$	
Lhasa	**3600**	**City**	**Southwest**	**8/2016-2/2017**	**2.26±1.97**	**36.4±48.9**	**54.5±119.5**				**This study**
Beijing	40	City	North china	12/2008-11/2009	3.22±1.74	10.1±18.8	98.2±112.7				(Zhang et al., 2013)
Hefei	30	City	East china	7/2013-6/2014	4.07±1.91	3.67±5.11	30.0±100.3				(Hong et al., 2016)
Shanghai	4	City	East china	2014	4.19±9.13	21±100	197±877				(Duan et al., 2017)
Lanzhou	1525	City	Northwest	10/2016-10/2017	4.48±2.32						(Yin et al., 2020)
Jinan	148	City	East china	10/2015 -7/2016	4.91±3.66		451.9±433.4				(Li et al., 2017)
Chongqing	300	City	Southwest	2006-2007	6.74±0.37						(Yang et al., 2009)
Nanjing	25	City	East china	2011	7.9±7.0						(Zhu et al., 2012)
Guiyang	1150	City	Southwest	8/2009-12/2009	9.72±10.2	35.7±43.9	368±676				(Liu et al., 2011)
Ev-K2, Nepal	5050	Remote		11/ 2011-4/2012	1.2±0.2			18/1.30	6/1.10	0.20	(Gratz et al., 2013)
Nam Co, China	5300	Remote		11/2014-3/2015	1.33±0.24						(Yin et al., 2018)
Waliguan, China	3816	Remote		9/2007-9/2008	1.98±0.98	7.4±4.8	19.4±18.1	6/2.30	14/1.94	0.36	(Fu et al., 2012b)
Shangri-La, China	3580	Remote		11/2009-11/2010	2.51±0.73	8.22±7.9	38.32±31.26	17/2.48	6/1.71	0.77	(Zhang et al., 2015a)
Gongga, China	1640	Remote		5/2005-6/2006	3.98			11/4.45	2/3.55	0.90	(Fu et al., 2008)
QNNP, China	4267	Remote		4/2016-8/2016	1.42±0.37	21.4±13.4	25.6±19.1	6/2.04	13/1.11	0.93	(Lin et al., 2019)
Nyingchi, China	3263	Remote		3/2019-9/2019	1.01±0.27	12.8±13.3	9.3±5.9	20/1.07	6/0.96	0.11	(Lin et al., 2022)

282   Compared to nearby monitoring stations (Table 2), Hg species concentrations in Lhasa were

283   high. Namco station is the nearest station; its altitude is 4,730 m and the distance between the two

284   stations is approximately 120 km. The GEM concentration in Namco was 1.33 ± 0.24 ng m^{-3}, which

285   was only 59% of Lhasa. This is likely because the Namco region is sparsely populated with minimal

286   local pollution and is far from major Hg pollution sources (Yin et al., 2018). Compared to the QNNP

287   (Lin et al., 2019) on Mt. Everest, which is approximately 500 km apart, the GEM, GOM, and PBM

288   concentrations in Lhasa were approximately 1.6, 1.7, and 2.1 times higher, respectively. Our

289   previous studies demonstrated that the QNNP is influenced by transported air masses from the

290   Indian subcontinent, indicating that the concentration in Lhasa is high in the Tibetan Plateau.

291   Compared to another typical highland site, Nyingchi, Lhasa had much high levels of atmospheric

292   Hg species, which may be related to the vegetation uptake effects and strong wet deposition in

293   Nyingchi (Lin et al., 2022). Among the surrounding stations, only Mt. Gongga and Shangri-La

294   stations had higher GEM concentrations than Lhasa. The GEM concentrations reported at Mt.

295   Gongga station ranged from May 2005 to July 2006. Considering that the smelting activities near

296   this site were crude at that time and there were almost no air pollution control measures, the high

297   local GEM concentrations may be strongly affected by local smelting activities and fuel combustion

298   (Fu et al., 2008). In contrast, GEM concentrations in the Shangri-La region were mainly controlled

299   by the monsoon, and Zhang et al. (2015a) suggested that all local GEM above 2.5 ng m^{-3} are

300   associated with the transport of dry air carrying domestic and foreign regional anthropogenic

301   emissions. Comparing these sites only for the monsoon period, the GEM concentration in Lhasa

302   was higher than that in the Shangri-La region. As for GOM and PBM, the concentrations at the

303   Lhasa station were much higher than those in the surrounding areas. The average GOM

304   concentration in the surrounding areas was approximately 10 pg m^{-3}, which was only 27% of that

305   in Lhasa, and the average PBM concentration in the surrounding areas was approximately 28 pg m^{-}

306   ^{3}, which was only 54% of that in Lhasa. Considering that GOM and PBM are mainly from local or

307   surrounding sources or atmospheric transport (Seigneur et al., 2006; Lynam et al., 2014; Lindberg

308   and Stratton, 1998), high GOM and PBM concentrations may indicate additional local sources of

309   Hg in Lhasa.

310   **3.2 Unexpected high concentration events in Lhasa**

311   To investigate the reasons for the random high atmospheric Hg concentration events in Lhasa,

312   typical high-value occurrence processes (defined as GEM concentrations above 10 ng m^{-3} monitored

313   more than five times on a single day) were selected for analysis in the S-ISM and WEC periods,

314   respectively. A total of seven high GEM concentration events were identified, of which, September

315   3, November 10, November 19, and December 9, 2016, were selected for analysis; September 18,

316   October 3, 2016, and January 27, 2017 were omitted due to lack of meteorological data or Hg

317   concentration data for the proximity date.

318   During the S-ISM period (Figure 2), there was a clear peak in Hg concentration on September

319   3, while the GEM, GOM, and PBM concentrations were approximately 1.6, 1.5, and 2.3 times the

320   average daily value, respectively. Comparing the two days before and after the high-concentration

321   event (Table 3, Figure 3. a), the concentrations of the three pollutants NO_2/$PM_{2.5}$/SO_2, were higher

322   on September 3. High GEM concentrations were accompanied by winds of 2.12 m/s from the

323   southwest, with NO_2 and SO_2 concentrations higher than usual as well as increased PBM

324   concentrations. NO_2 and SO_2 are typical combustion source pollutants, and the presence of $PM_{2.5}$,

325   and PBM may indicate more combustion sources in the day. Thus, it can be inferred that the elevated

326   Hg concentration event on September 3 may have originated mainly from a combustion event

327   nearby or further away.

328   During the WEC period, significantly high values were observed on November 10, November

329   19, and December 9. On November 10 (Figure 3.b), the increase in atmospheric Hg species

330   concentrations was accompanied by significant increases in CO/NO_2/PM_{10}/$PM_{2.5}$/SO_2

331   concentrations. Two similar peaks in atmospheric Hg species concentrations were also observed

332   around November 10, with relatively lower peak concentrations. During these three events, the

333   concentrations of other pollutants were higher than usual, whereas wind speeds were extremely low

334   during the event periods. In addition, extremely high PBM concentrations (297.7±189.3 pg m^{-3},

335   maximum 621.2 pg m^{-3}) were observed at midnight on November 12 which, considering the

336   extremely low wind speed and the presence of a low height nocturnal boundary layer, may indicate

337   that the high concentrations originated from local sources.

Table 3 Comparation of the pollutant concentrations with the two days before and after the high Hg concentration events

Item		9.1-2	9.3	9.4-5	11.8-9	11.10	11.11-12	11.17-18	11.19	11.20-21	12.7-8	12.9	12.10-11
GEM	(ng m^{-3})	2.72	**4.63**	3.03	1.47	**3.16**	**2.96**	2.15	**6.87**	2.66	2.76	**5.43**	3.24
PBM	(pg m^{-3})	25.32	**64.17**	31.52	36.31	**47.21**	**94.80**	53.41	**74.78**	55.40	38.71	**66.74**	49.05
GOM	(pg m^{-3})	40.95	**63.84**	42.55	32.76	**39.48**	**42.03**	35.29	**119.39**	44.86	43.84	**69.65**	43.75
Temp.	(°C)	16.61	15.86	15.32	7.06	7.76	8.80	4.20	4.49	4.94	3.13	2.88	2.77
Hum.	(%)	58.47	67.89	68.71	19.96	22.02	21.04	21.82	23.35	25.67	23.50	26.86	26.09
Wind	(m s^{-1})	2.37	1.46	1.49	1.47	**0.93**	1.17	1.05	**0.71**	0.75	0.88	0.89	0.67
Barometer	(hPa)	651.62	651.08	652.39	654.90	654.33	652.31	655.11	652.18	653.57	657.99	655.66	653.08
rainfall	(mm)	0.01	0.17	0.36	0.00	0.00	0.00	0.00	0.00	0.00	0.00	0.00	0.00
Solar Rad.	(W m^{-2})	241.20	201.15	214.39	189.02	194.45	182.30	166.14	161.59	180.02	141.61	139.69	136.64
CO	(mg m^{-3})	0.34	**0.36**	0.32	0.39	**0.76**	**0.63**	0.64	0.71	0.72	0.67	0.80	0.74
NO$_2$	(μg m^{-3})	20.44	**26.00**	21.77	41.38	**57.64**	**66.48**	54.58	53.58	55.27	48.87	55.33	56.23
O$_3$	(μg m^{-3})	85.73	77.42	72.56	59.27	57.43	49.46	34.73	34.79	29.51	31.37	28.38	26.81
PM$_{10}$	(μg m^{-3})	33.90	32.78	26.95	80.71	**130.07**	**155.44**	107.98	**119.79**	146.29	125.82	137.74	143.13
PM$_{2.5}$	(μg m^{-3})	11.98	**17.10**	10.98	31.20	**75.07**	**64.85**	51.21	50.13	53.83	62.80	65.46	62.71
SO$_2$	(μg m^{-3})	4.23	**5.89**	4.91	3.83	**6.07**	**5.71**	6.50	**8.92**	**9.44**	6.00	6.88	6.69

338

339   On November 19 (Figure 3.c), there was a significant increase in all atmospheric Hg species

340   concentrations. During the elevated period, the average GEM, GOM, and PBM concentrations were

341   17.94±10.54 ng m^{-3}, 302.5±218.5 pg m^{-3}, and 162.4±54.0 pg m^{-3}, respectively, which were 8.3, 5.7,

342   and 4.6 times higher than the average concentrations on November 17-18. However, only a slight

343   increase in the peak CO/ $PM_{2.5}$/SO_2 concentration was observed during the event period. Therefore,

344   the increase in atmospheric Hg species concentrations may indicate that this event was unique, with

345   certain sources of high Hg concentrations. The low wind speed and low nocturnal boundary layer

346   height both contributed to the accumulation of atmospheric Hg species, which also indicated that

347   the elevated Hg was from local sources. Similar to the event on November 19, sharp increases in

348   atmospheric Hg species concentrations were observed only on December 9 (Figure 3.d). The

349   atmospheric Hg species concentration increase events during the WEC period occurred at night and,

350   given that it coincided with the winter heating period, local combustion sources may be the unique

351   sources that may contribute to the Hg concentration increase.
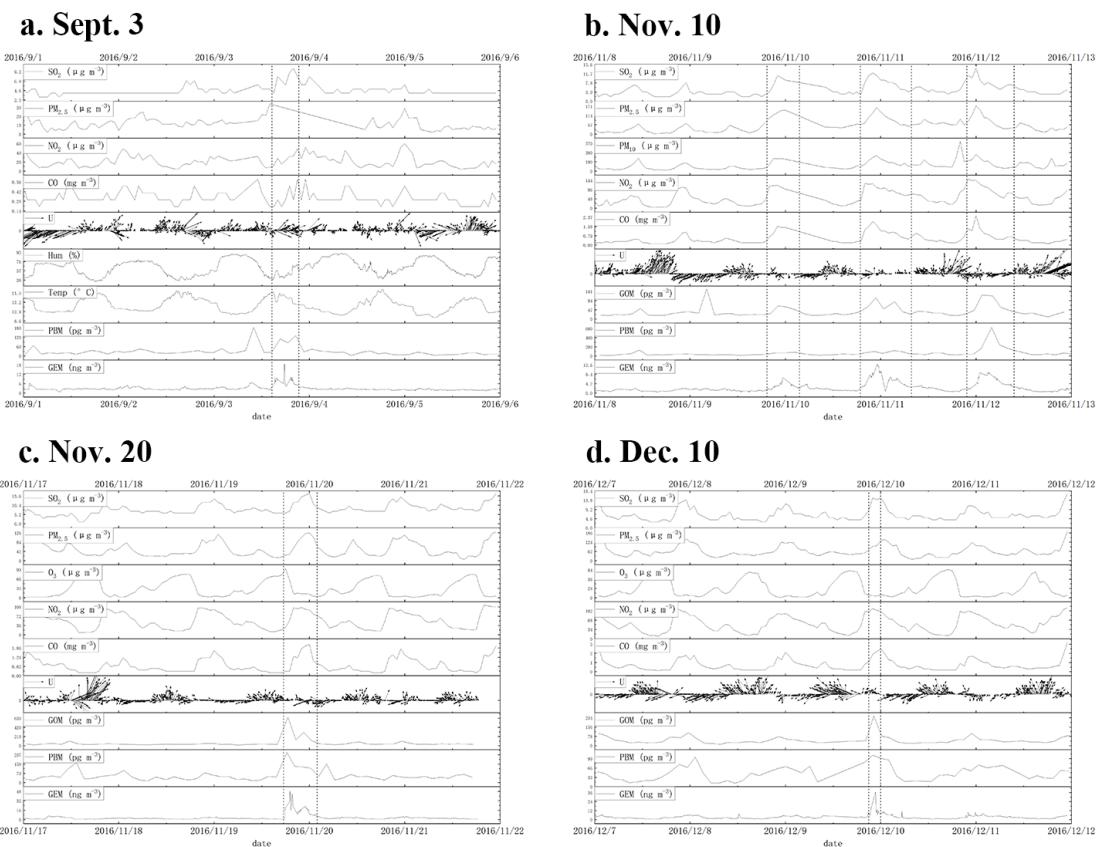
352

353   **Figure 3 Comparison of the pollutant concentrations with those at the two days before and**

354   **after the high Hg concentration events. The dotted lines indicate the area where the Hg**

355   **concentrations are significantly elevated**

356   **3.3 Diurnal variation of atmospheric Hg in Lhasa**

357   Figure 4.a shows the diurnal variation of atmospheric Hg in Lhasa during the monitoring period.

358   The mean GEM concentration during this period was 2.26±1.97 ng m^{-3}, and the maximum

359   difference of hourly average GEM diurnal variation was 1.89 ng m^{-3}. GEM concentration was low

360   during the day; the lowest concentration of the day appeared from 14:00-18:00 (UTC+8). The GEM

361   concentration kept increasing and reached the peak at midnight. During the night, the GEM

362   concentration maintained in high value with little dissipation. Subsequently, the GEM concentration

363   decreased rapidly with the sunrise. Overall, the diurnal variation of GEM concentration was similar

364   to CO, NO$_2$, and relative humidity, and opposite to O$_3$ and wind speed. The high GEM

365   concentrations at night can be attributed to the lower boundary layer height at night (average at 131

366   m a.g.l. during the observation period, between 19:00 and 07:00, UTC+8) and the lower wind speed

367   (Figure 4). Also, the average night temperature in Lhasa during the monitoring period was 5.8°C,

368   and the residents heating combustion may bring about the release of GEM. After sunrise, the

369   boundary layer height increased rapidly and the diffusion quickly occurred in the lower atmosphere.

370   During the increase of wind speed, airflows were carried from other regions with few populations,

371   which may lead to a decrease in GEM concentrations. For both GOM and PBM, the higher GOM

372   concentrations occurred during the day and higher PBM concentration occurred during the night.

373   No obvious increase occurred for GOM and PBM concentrations at the same time, which may

374   indicate that there is no local common external source, and the variation of GOM and PBM

375   concentrations may come from the gas-particle redistribution process of atmospheric Hg(II).

376
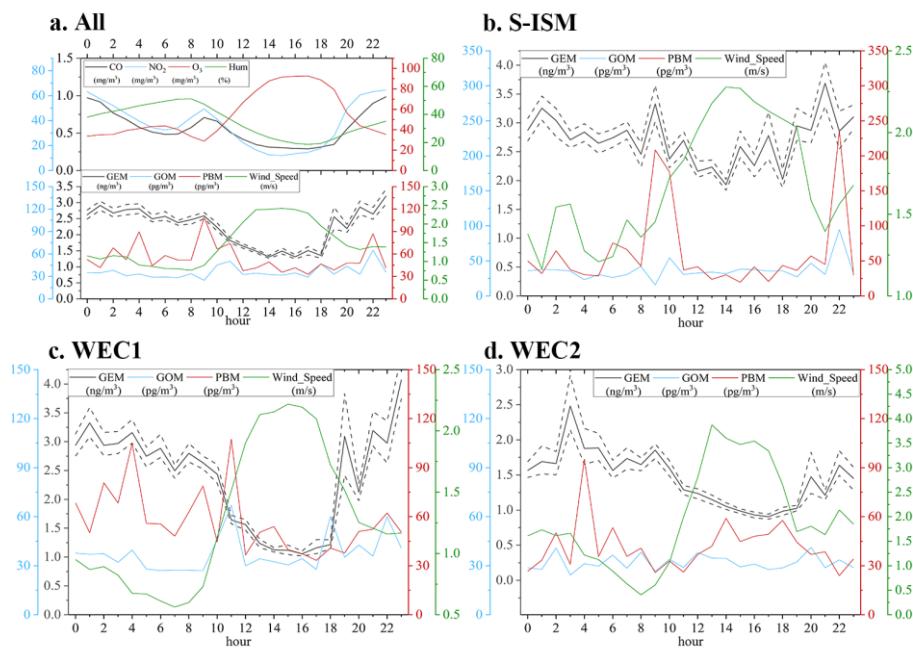
    Figure 4 Diurnal variations of Hg species, concentrations of other pollutants, and

    meteorological information from S-ISM to WEC periods. The short horizontal line

    represents the concentration error range for each time period.

380   In particular, during the S-ISM period (Figure 4.b), the diurnal variation in GEM

381 concentrations fluctuated frequently, which indicates that the factors affecting the concentration

382 variation were very complicated. The mean concentration of GEM during this period was 2.73 ng

383 m^{-3}, and the maximum difference of GEM diurnal variation was 1.40 ng m^{-3}. September was the

384 ending period of the Indian summer monsoon, and the external transboundary transport of air masses

385 by the monsoon may have been weakened. Simultaneously, the average temperature in September

386 was high (14.4°C) without residents heating during the night, which may be the reason for the small

387 diurnal variation in GEM concentrations. Overall, GEM concentrations remained lower during the

388 day, increased, and remained high at night. No clear pattern of variation was observed in GOM and

389 PBM during this period.

390   During the WEC1 period, the diurnal variation in GEM concentrations was exceedingly large.

391 The mean GEM value was 2.39 ng m^{-3} with great GEM diurnal variation value (3.01 ng m^{-3}). The

392 diurnal trend was roughly the same as the whole monitoring period, but the lowest value was 1.06

393 ng m^{-3} and the highest value was 4.07 ng m^{-3}. The increase in night concentrations may be related

394 to the beginning of the heating season, whereas the burning of yak dung, firewood, or other fuels

395 for residential heating may release GEM and PBM, and accumulate within the boundary layer at

396 night, leading to higher GEM concentrations (Rhode et al., 2007; Xiao et al., 2015; Chen et al.,

397 2015). In contrast, low day values may be related to the wind field. Although the wind speed during

398 the WEC1 period was similar to that during the S-ISM period, westerly circulation was prevalent in

399 Lhasa during the WEC1 period, with air masses coming from the sparsely populated area with lower

400 GEM concentrations. The westerly winds carry away the locally accumulated GEM air masses in

401 Lhasa and bring in low GEM concentration air masses from west of Lhasa. During this period, the

402 diurnal variation in GOM concentrations was not clear.

403   The influence of wind flow was evident during the WEC2 period. During this period, GEM

404 concentrations in Lhasa were the lowest and close to 1.00 ng m^{-3} in the late afternoon when wind

405 speeds were the highest. Nighttime concentrations were lower in the WEC2 period than in the

406 WEC1 period, probably because wind speeds were also high at night during the WEC2 period

407 (19:00-4:00 UTC+8, mean wind speed 1.74 m/s). The heating season was still in progress during

408 the WEC2 period, but GEM emissions from heating were likely carried away by the continuous

409 flow of air masses. Therefore, the mean GEM concentration in Lhasa during the winter was likely

410 strongly influenced by wind speed.

411   Compared to the diurnal variation patterns obtained from monitoring in other remote areas of

412 China (Figure S3), the diurnal variation of GEM in Lhasa is more unique, and a wide diurnal

413 variation in concentration was observed. Valleys of GEM concentrations in the afternoon were also

414 observed in Waliguan and Namco, but the concentration variation ranges were small in both areas.

415 This could be related to the regional characteristics of the three sites. Waliguan is located in a

416 mountainous area with no significant local anthropogenic sources, and is mainly influenced by

417 valley winds (Fu et al., 2012b). Namco is located in the central Tibetan region away from

418 anthropogenic sources. Although the wind speed was also high in the afternoon in Namco (Yin et

419 al., 2018), it is likely that the diurnal variation in atmospheric GEM concentrations was small

420 because the atmosphere was well-proportioned and there were no local sources; therefore, the

421 changes in wind speed might not affect the GEM concentration. In contrast, with the difference in

422 GEM concentrations between Lhasa and the transmitted external air mass, wind speed could

423 significantly influence the GEM concentrations in Lhasa. Meteorological conditions may have

424 played a more important role. We conjecture that the high nighttime concentrations in Lhasa may

425 originate mainly from local emissions, while the high wind speed and mixing of clean external air

426 masses in the afternoon reduce the local GEM concentrations.

427   **3.4 Analysis of factors affecting atmospheric Hg concentration in Lhasa**

428   Overall, four principal components were obtained for each period, from S-ISM to WEC2, using

429 PCA analyze, to analyze the relationships between Hg and multiple pollutants and meteorological

430 variables. The Hg monitoring data, meteorological factors, and pollutant data in Lhasa were

431 statistically and dimensionally reduced by PCA to analyze the relationships among them. The

432 components related to Hg were selected and analyzed separately for each period, and the principal

433 components were extracted (Table 4). According to the variable's loadings on each component, they

434 were assigned as Special Hg-related factor, Local emission factor, and Wind factor.

Table 4 PCA factor loadings (varimax rotated factor matrix) for Hg in Lhasa, China.

Tentative Identification	Special Hg-related			Local emission		Wind	
preiod	S-ISM	WEC1	WEC2	WEC1	WEC2	S-ISM	WEC2
GEM	**0.87**	**0.63**	**0.9**	0.44	0.3	-0.21	-0.13
PBM	**0.96**	**0.79**	**0.63**				
GOM	**0.95**	**0.87**	**0.95**	0.11	0.1		
Temp				-0.29	0.2		**0.92**
Hum		-0.19	0.17	-0.26	-0.18	-0.26	**-0.75**
Wind_Speed	-0.1	-0.14		-0.37		**0.87**	**0.91**
Rain							
Solar_Rad.				-0.21			
CO	0.17		0.11	**0.87**	**0.69**	-0.22	**0.51**
NO$_2$		0.13		**0.92**	**0.96**	-0.25	
O$_3$			-0.36	**-0.89**	**-0.83**	0.53	
PM$_{10}$	-0.14			**0.86**	**0.69**		0.14
PM$_{2.5}$	-0.16		0.16	**0.83**	**0.86**		
SO$_2$	0.26	0.17	**0.86**	**0.75**			
Variance Explained	19.6	13.69	21.88	35.13	24.94	9.25	18.32

Note:variables with high factor loadings (> 0.5) were marked in bold. For readability, variables with very low factor loadings (< 0.1) are not presented.

435

436  A special Hg-related factor (Factor 1) was assigned owing to the continuous high positive

437 loading of GEM, GOM, and PBM from the SISM to the WEC periods; only high positive loading

438 of SO$_2$ was found in the WEC2 period. For this factor, there was no significant relationship with

439 any other meteorological factors or pollutants. The high positive loading of this factor for all three

440 Hg species and the low correlation with meteorological factors and other pollutants may indicate

441 that this is a specific source of Hg. As the short transmission distance of the GOM and PBM, the

442 special Hg-related source should be closer to Lhasa. However, no particular source of Hg around

443 Lhasa has been reported in the literature, so the source indicated by this factor remains unclear.

444  Factor 2 had slight positive relationship with GEM and GOM, high positive loading of

445 CO/NO$_2$/PM$_{10}$/PM$_{2.5}$/SO$_2$, and high negative loading of O$_3$ during the WEC period. The high

446 positive loadings of CO/NO$_2$/PM$_{10}$/PM$_{2.5}$/SO$_2$ may indicate that this factor is highly correlated with

447 the combustion source. As O$_3$ concentration rapidly decreased after sunset (Figure 4. a), high

448 negative loading of O$_3$ further indicated that this factor represented events during the nighttime with

449   low O_3 concentrations. Since the WEC period overlapped with the heating season in Lhasa, Factor

450   2 may be strongly associated with heating combustion.

451   The wind factor (Factor 3) involves high positive loading of wind speed and low negative

452   loading of GEM concentration during the S-ISM and WEC2 periods. This factor reveals the

453   scavenging effect of wind on the local GEM in Lhasa. For high wind speed, the air masses with low

454   GEM concentrations in the surrounding area mixed with the air masses in Lhasa, leding to a

455   reduction in the GEM concentration. Concurrently, some GEM in Lhasa was carried away from the

456   city by wind. At wind speed greater than 4m s^{-1}, the average GEM concentration in Lhasa was

457   1.31 ± 0.93 ng m^{-3}, which is similar to the average concentration of Nam Co (1.33 ± 0.24 ng m^{-3}) in

458   the Tibetan hinterland. Factor 3 was consistent with the analysis of the wind effect on the diurnal

459   variation of Hg concentrations (Section 3.2), indicating the effect of strong winds on urban Hg

460   removal.

461   **3.5   Atmospheric Hg source trajectories and potential source regions in the Lhasa area**

462   Figure 4 shows the GEM backward trajectory paths from the S-ISM period to the WEC2 period

463   in Lhasa. During the S-ISM period, most trajectories (cluster 1, representative GEM concentration

464   of 2.66 ng m^{-3}, 87.53% of the trajectory during this period, Table S1) originated from or passed

465   through the south of Lhasa. The source of the trajectory points directly to the Indian Ocean, likely

466   as these transported air masses are still subject to Indian monsoon action in September. According

467   to the UNEP Hg emission inventory (Unep, 2013), there are few anthropogenic emissions along this

468   trajectory, indicating that the GEM may originate from the Indian Ocean or locally from Lhasa.

469   Clusters 2 and 3 may indicate the trajectories of air masses driven by westerly circulation, which

470   had a low proportion in the S-ISM period, with slightly different GEM concentrations from different

471   sources.

472   During the WEC1 period, the driving factor of the air mass gradually shifted from Indian

473   monsoon to westerly circulation. Clusters 2 and 3 are trajectories driven by the higher-height

474   westerly circulation during the WEC1 period with a higher proportion than in the S-ISM period.

475   Cluster 1 came from the southwest of Lhasa, and the air mass moved along the Himalayas before

476   entering the Tibetan Plateau and was transported to Lhasa. Compared to the S-ISM period, the GEM

477   concentration of this trajectory decreased slightly, which may be related to the source of the air mass

478   and the areas it passes through. WEC2 showed little change in trajectory sources compared to WEC1,

479   but all trajectory concentrations decreased significantly. Both WEC1 and WEC2 were in winter,

480   and both had similar trajectories related to the driving wind field. Significantly decreasing GEM

481   concentrations may suggest a local influence in Lhasa City. The local GEM in Lhasa consists of

482   background concentrations superimposed on local emissions, and the share of local emissions

483   decreases under better dispersion conditions (higher wind speeds) during the WEC2 period. The

484   GEM concentration during the WEC2 period in Lhasa was only 0.16 ng m^{-3} higher than that during

485   the WEC period in the QNNP region (1.31 ± 0.42 ng m^{-3}) (Lin et al., 2019)).

486
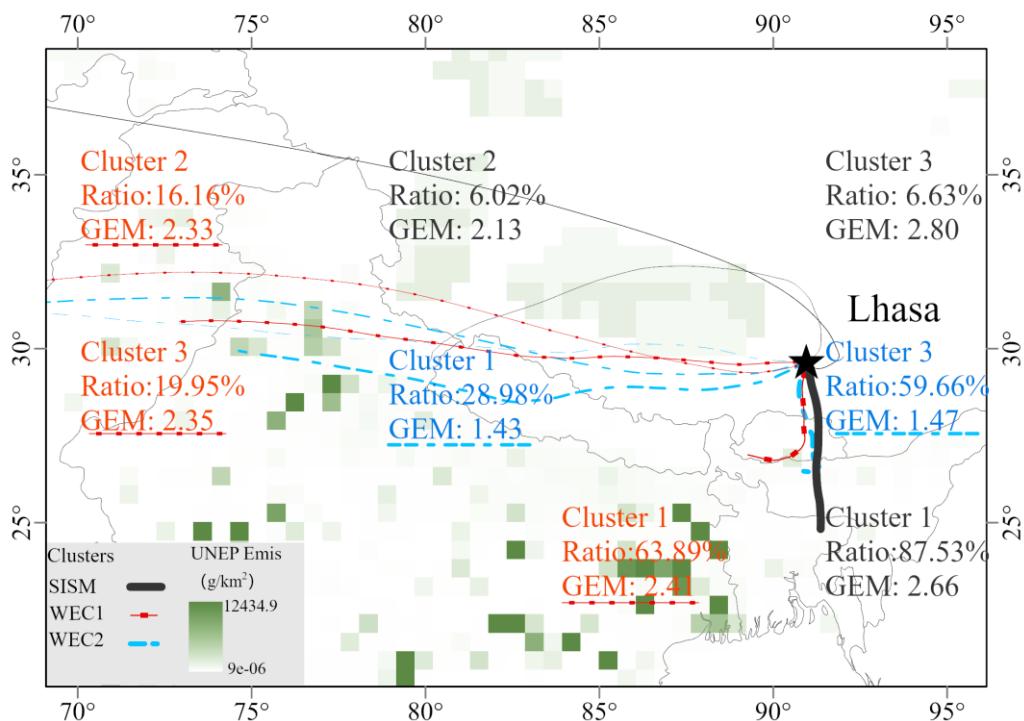
487   **Figure 5 Clusters of the back trajectory analysis from Lhasa during S-ISM and WEC**

488   **periods. The thickness of the line represents the ratio of the cluster in the time period, the**

489   **background is the global Hg emission inventory developed by UNEP (2013a).**

490   **3.6 Comparison of three typical sites on the Tibetan Plateau**

491   Different levels and variation patterns of Hg species concentrations were observed in the

492   Qomolangma National Nature Preserve (QNNP, 4,276 m) (Lin et al., 2019), Nyingchi (SET, 3,263

493   m) (Lin et al., 2022), and Lhasa (3,650 m) areas, which are typical monsoon-influenced, canyon,

494   and urban areas on the Tibetan Plateau, respectively. Predictably, Hg species concentrations were

generally lower on the Tibetan Plateau, while background areas with few populations on the Plateau were lower than those on the plains in mainland China, and cities on the Plateau were lower than those on the plains. Although the transboundary transport of pollutants has received considerable notice (Huang et al., 2016b; Wang et al., 2018; Lin et al., 2019; Zhu et al., 2019; Feng et al., 2019), the comparison between QNNP and Lhasa indicates that the contribution of local anthropogenic sources may be significant for atmospheric pollutant concentrations. The comparison also suggests that atmospheric Hg emissions from urban residential life may be an important source that can be valuable in inventory studies.

Vastly different patterns of Hg species concentrations were found in the QNNP and SET due to differences in geography and vegetation cover. Atmospheric Hg transported to QNNP is subject to a combination of monsoonal action and the pumping effect of glacial winds. However, atmospheric Hg entering the SET area has a slow elevation increasing path, and abundant precipitation and vegetation have a significant trapping effect on atmospheric Hg. While for Lhasa, a direct effect of local wind fields on the accumulation or rapid removal of GEM concentrations was found. This suggests that although global transport is important in the Hg cycle, the pollution at each location is likely to be strongly influenced by the local environment, even in exceptionally clean areas such as the Tibetan Plateau. However, there are still relatively few studies on GOM and PBM in the Tibetan Plateau, and more comprehensive investigations are required on how changes in Hg speciation transformation on snow and ice surfaces affect the environment, the effect of stratospheric intrusion on GOM concentrations (which is common on the Plateau), and the effect of particulate matter on Hg(II) gas-particle partitioning, which would help to understand the Hg species change on the Plateau and throughout the world.

4. Conclusions

Lhasa is the largest city on the Tibetan Plateau; thus, its atmospheric Hg concentrations represent the highest level of atmospheric Hg pollution in this area. Unexpectedly high concentrations of atmospheric Hg species were found in Lhasa. The GEM concentrations were higher than the Northern Hemisphere background concentrations, and the GOM and PBM concentrations were high among Chinese cities. Monitoring of atmospheric Hg in Lhasa showed that the mean concentrations of GEM, GOM, and PBM during the S-ISM period (2.73 ± 1.48 ng m^{-}

524 ^{3}, 38.4 ± 62.7 pg m^{-3}, and 59.1 ± 181.0 pg m^{-3}, respectively) were higher than those during the WEC

525 period (2.11 ± 2.09 ng m^{-3}, 35.8 ± 43.3 pg m^{-3}, and 52.9 ± 90.1 pg m^{-3}, respectively). Combined

526 with the trajectory analysis, the high atmospheric Hg concentrations during the S-ISM phase may

527 have originated from external long-range transport.

528   Analysis of the overall concentration changes revealed some irregular and sudden high

529 atmospheric Hg concentration events in Lhasa. Analysis of these events suggests that local sources

530 (such as combustion events) can cause severely elevated concentration events under low wind

531 speeds and the presence of a low-height nighttime boundary layer. Analysis of the diurnal variation

532 of concentrations confirmed that low wind speeds and a low height nocturnal boundary layer would

533 lead to the elevated local Hg concentrations. In contrast, higher wind speeds could rapidly remove

534 atmospheric Hg from Lhasa. PCA analysis of the influencing factors indicates that local sources,

535 especially special Hg-related sources, are important factors influencing the variability of

536 atmospheric Hg. The PCA analysis also indicated the important role of higher wind speeds in

537 reducing atmospheric Hg concentrations in the urban areas of Lhasa, likely owing to the large Hg

538 concentration difference between Lhasa and surrounding areas.

539   Up to this study, we have obtained atmospheric Hg monitoring data from four typical areas of

540 the Tibetan Plateau: Lhasa, QNNP, SET, and Namco. The atmospheric Hg concentrations in the

541 background areas were at or below the average GEM concentration of Northern Hemisphere, with

542 higher levels in the urban area of Lhasa. Factors such as long-range transport of atmospheric Hg,

543 effects of local meteorological conditions, local glaciers, etc., were considered in these studies.

544 Further monitoring of additional areas and regional simulations are required to confirm the

545 atmospheric Hg transport patterns and fluxes.

546

547   **Acknowledgments**

548 This study was funded by the National Natural Science Foundation of China (Grant #41821005,

549 41977311, 42122059, 41907328). The authors are grateful to NOAA for providing the HYSPLIT

550 model and GFS meteorological files. We also thank the staffs of Lhasa station of the Institute of

551 Tibetan Plateau Research, Chinese Academy of Sciences on Lhasa for field sampling assistance.

552   **Data availability.** All the data presented in this paper can be made available for scientific

553   purposes upon request to the corresponding authors.

554   **Author contributions.** HL,XW, YT, QZ and XY designed the research and performed field

555   measurements. HL and YT performed the data analysis and model simulations. HL led the paper

556   writing. LC,CY, ZC, QZ, SK, JL, JS and BF contributed to the scientific discussion and the paper

557   preparation.

558   **Competing interests.** The authors declare that they have no conflict of interest.

559

References

Brooks, S., Luke, W., Cohen, M., Kelly, P., Lefer, B., and Rappenglück, B.: Mercury species measured atop the Moody Tower TRAMP site, Houston, Texas, Atmospheric Environment, 44, 4045-4055, 10.1016/j.atmosenv.2009.02.009, 2010.

Chai, T., Stein, A., Ngan, F., and Draxler, R.: Inverse modeling with HYSPLIT Lagrangian Dispersion Model-Tests and Evaluation using the Cross Appalachian Tracer Experiment (CAPTEX) data, AGU Fall Meeting Abstracts,

Chai, T., Crawford, A., Stunder, B., Pavolonis, M. J., Draxler, R., and Stein, A.: Improving volcanic ash predictions with the HYSPLIT dispersion model by assimilating MODIS satellite retrievals, Atmospheric Chemistry and Physics, 17, 2865-2879, 10.5194/acp-17-2865-2017, 2017.

Chen, P., Kang, S., Bai, J., Sillanpää, M., and Li, C.: Yak dung combustion aerosols in the Tibetan Plateau: Chemical characteristics and influence on the local atmospheric environment, Atmospheric Research, 156, 58-66, 10.1016/j.atmosres.2015.01.001, 2015.

Cheng, I., Zhang, L., Blanchard, P., Graydon, J. A., and Louis, V. L. S.: Source-receptor relationships for speciated atmospheric mercury at the remote Experimental Lakes Area, northwestern Ontario, Canada, Atmospheric Chemistry and Physics, 12, 1903-1922, 10.5194/acp-12-1903-2012, 2012.

Ci, Z., Zhang, X., Wang, Z., and Niu, Z.: Atmospheric gaseous elemental mercury (GEM) over a coastal/rural site downwind of East China: Temporal variation and long-range transport, Atmospheric Environment, 45, 2480-2487, 10.1016/j.atmosenv.2011.02.043, 2011.

Cong, Z., Kang, S., Luo, C., Li, Q., Huang, J., Gao, S., and Li, X.: Trace elements and lead isotopic composition of PM10 in Lhasa, Tibet, Atmospheric Environment, 45, 6210-6215, 10.1016/j.atmosenv.2011.07.060, 2011.

Dommergue, A., Ferrari, C. P., Gauchard, P.-A., Boutron, C. F., Poissant, L., Pilote, M., Jitaru, P., and Adams, F. C.: The fate of mercury species in a sub-arctic snowpack during snowmelt, Geophysical Research Letters, 30, 10.1029/2003gl017308, 2003.

Duan, L., Wang, X., Wang, D., Duan, Y., Cheng, N., and Xiu, G.: Atmospheric mercury speciation in Shanghai, China, The Science of the total environment, 578, 460-468, 10.1016/j.scitotenv.2016.10.209, 2017.

Feng, Wang, and Liu: Dilemmas in and Pathways to Transboundary Water Cooperation between China and India on the Yaluzangbu-Brahmaputra River, Water, 11, 2096, 10.3390/w11102096, 2019.

Feng, X., Fu, X., and Zhang, H.: Observations of atmospheric Hg species and depositions in remote areas of China, E3S Web of Conferences, 10.1051/e3sconf/20130107001,

Fu, X., Feng, X., Sommar, J., and Wang, S.: A review of studies on atmospheric mercury in China, The Science of the total environment, 421-422, 73-81, 10.1016/j.scitotenv.2011.09.089, 2012a.

Fu, X., Feng, X., Zhu, W., Wang, S., and Lu, J.: Total gaseous mercury concentrations in ambient air in the eastern slope of Mt. Gongga, South-Eastern fringe of the Tibetan plateau, China, Atmospheric Environment, 42, 970-979, 10.1016/j.atmosenv.2007.10.018, 2008.

Fu, X., Feng, X., Liang, P., Zhang, H., Ji, J., and Liu, P.: Temporal trend and sources of speciated atmospheric mercury at Waliguan GAW station, Northwestern China, Atmospheric Chemistry and Physics, 12, 1951-1964, 2012b.

Fu, X., Zhang, H., Feng, X., Tan, Q., Ming, L., Liu, C., and Zhang, L.: Domestic and Transboundary Sources of Atmospheric Particulate Bound Mercury in Remote Areas of China: Evidence from Mercury Isotopes, Environ Sci Technol, 53, 1947-1957, 10.1021/acs.est.8b06736, 2019.

604 Fu, X., Zhu, W., Zhang, H., Sommar, J., Yu, B., Yang, X., Wang, X., Lin, C.-J., and Feng, X.: Depletion
605 of atmospheric gaseous elemental mercury by plant uptake at Mt.
606 Changbai, Northeast China, Atmospheric Chemistry and Physics, 16, 12861-12873, 10.5194/acp-
607 16-12861-2016, 2016.
608 Gay, D. A., Schmeltz, D., Prestbo, E., Olson, M., Sharac, T., and Tordon, R.: The Atmospheric Mercury
609 Network: measurement and initial examination of an ongoing atmospheric mercury record across
610 North America, Atmospheric Chemistry and Physics, 13, 11339-11349, 10.5194/acp-13-11339-
611 2013, 2013.
612 Gratz, L., Esposito, G., Dalla Torre, S., Cofone, F., Pirrone, N., and Sprovieri, F.: First Measurements
613 of Ambient Total Gaseous Mercury (TGM) at the EvK2CNR Pyramid Observatory in Nepal, E3S Web
614 of Conferences,   10.1051/e3sconf/20130127004,
615 Guo, J., Kang, S., Huang, J., Zhang, Q., Tripathee, L., and Sillanpää, M.: Seasonal variations of trace
616 elements in precipitation at the largest city in Tibet, Lhasa, Atmospheric Research, 153, 87-97,
617 10.1016/j.atmosres.2014.07.030, 2015.
618 Hong, Q., Xie, Z., Liu, C., Wang, F., Xie, P., Kang, H., Xu, J., Wang, J., Wu, F., He, P., Mou, F., Fan, S.,
619 Dong, Y., Zhan, H., Yu, X., Chi, X., and Liu, J.: Speciated atmospheric mercury on haze and non-
620 haze days in an inland city in China, Atmospheric Chemistry and Physics, 16, 13807-13821,
621 10.5194/acp-16-13807-2016, 2016.
622 Horowitz, H. M., Jacob, D. J., Zhang, Y., Dibble, T. S., Slemr, F., Amos, H. M., Schmidt, J. A., Corbitt,
623 E. S., Marais, E. A., and Sunderland, E. M.: A new mechanism for atmospheric mercury redox
624 chemistry: Implications for the global mercury budget, Atmospheric Chemistry and Physics, 17,
625 6353-6371, 10.5194/acp-17-6353-2017, 2017.
626 Hu, Q. H., Kang, H., Li, Z., Wang, Y. S., Ye, P. P., Zhang, L. L., Yu, J., Yu, X. W., Sun, C., and Xie, Z. Q.:
627 Characterization of atmospheric mercury at a suburban site of central China from wintertime to
628 springtime, Atmospheric Pollution Research, 5, 769-778, 10.5094/apr.2014.086, 2014.
629 Huang, J., Kang, S., Shen, C., Cong, Z., Liu, K., Wang, W., and Liu, L.: Seasonal variations and sources
630 of ambient fossil and biogenic-derived carbonaceous aerosols based on 14C measurements in
631 Lhasa, Tibet, Atmospheric Research, 96, 553-559, 10.1016/j.atmosres.2010.01.003, 2010.
632 Huang, J., Kang, S., Guo, J., Zhang, Q., Cong, Z., Sillanpää, M., Zhang, G., Sun, S., and Tripathee, L.:
633 Atmospheric particulate mercury in Lhasa city, Tibetan Plateau, Atmospheric Environment, 142,
634 433-441, 10.1016/j.atmosenv.2016.08.021, 2016a.
635 Huang, J., Kang, S., Tian, L., Guo, J., Zhang, Q., Cong, Z., Sillanpää, M., Sun, S., and Tripathee, L.:
636 Influence of long-range transboundary transport on atmospheric water vapor mercury collected
637 at the largest city of Tibet, Science of The Total Environment, 566, 1215-1222,
638 10.1016/j.scitotenv.2016.05.177, 2016b.
639 Huang, J., Kang, S., Wang, S., Wang, L., Zhang, Q., Guo, J., Wang, K., Zhang, G., and Tripathee, L.:
640 Wet deposition of mercury at Lhasa, the capital city of Tibet, The Science of the total environment,
641 447, 123-132, 10.1016/j.scitotenv.2013.01.003, 2013.
642 Hurst, T. and Davis, C.: Forecasting volcanic ash deposition using HYSPLIT, Journal of Applied
643 Volcanology, 6, 5, 10.1186/s13617-017-0056-7, 2017.
644 Jackson, J. E.: A user's guide to principal components, John Wiley & Sons2005.
645 Jiskra, M., Sonke, J. E., Obrist, D., Bieser, J., Ebinghaus, R., Myhre, C. L., Pfaffhuber, K. A., Wängberg,
646 I., Kyllönen, K., and Worthy, D.: A vegetation control on seasonal variations in global atmospheric
647 mercury concentrations, Nat Geosci, 11, 244-250, 10.1038/s41561-018-0078-8, 2018.

Kellerhals, M., Beauchamp, S., Belzer, W., Blanchard, P., Froude, F., Harvey, B., McDonald, K., Pilote, M., Poissant, L., Puckett, K., Schroeder, B., Steffen, A., and Tordon, R.: Temporal and spatial variability of total gaseous mercury in Canada: results from the Canadian Atmospheric Mercury Measurement Network (CAMNet), Atmospheric Environment, 37, 1003-1011, 10.1016/s1352-2310(02)00917-2, 2003.

Lan, X., Talbot, R., Castro, M., Perry, K., and Luke, W.: Seasonal and diurnal variations of atmospheric mercury across the US determined from AMNet monitoring data, Atmospheric Chemistry and Physics, 12, 10569-10582, 10.5194/acp-12-10569-2012, 2012.

Li, C., Chen, P., Kang, S., Yan, F., Hu, Z., Qu, B., and Sillanpää, M.: Concentrations and light absorption characteristics of carbonaceous aerosol in PM 2.5 and PM 10 of Lhasa city, the Tibetan Plateau, Atmospheric Environment, 127, 340-346, 10.1016/j.atmosenv.2015.12.059, 2016a.

Li, C., Bosch, C., Kang, S., Andersson, A., Chen, P., Zhang, Q., Cong, Z., Chen, B., Qin, D., and Gustafsson, O.: Sources of black carbon to the Himalayan-Tibetan Plateau glaciers, Nat Commun, 7, 12574, 10.1038/ncomms12574, 2016b.

Li, J., Lin, T., Qi, S., Zhang, G., Liu, X., and Li, K.: Evidence of local emission of organochlorine pesticides in the Tibetan plateau, Atmospheric Environment, 42, 7397-7404, 10.1016/j.atmosenv.2008.06.030, 2008.

Li, Y., Wang, Y., Li, Y., Li, T., Mao, H., Talbot, R., Nie, X., Wu, C., Zhao, Y., Hou, C., Wang, G., Zhou, J., and Qie, G.: Characteristics and potential sources of atmospheric particulate mercury in Jinan, China, The Science of the total environment, 574, 1424-1431, 10.1016/j.scitotenv.2016.08.069, 2017.

Lin, H., Tong, Y., Yu, C., Chen, L., Yin, X., Zhang, Q., Kang, S., Luo, L., Schauer, J., de Foy, B. J. A. C., and Physics: First observation of mercury species on an important water vapor channel in the southeastern Tibetan Plateau, 22, 2651-2668, 10.5194/acp-22-2651-2022, 2022.

Lin, H., Tong, Y., Yin, X., Zhang, Q., Zhang, H., Zhang, H., Chen, L., Kang, S., Zhang, W., Schauer, J., de Foy, B., Bu, X., and Wang, X.: First measurement of atmospheric mercury species in Qomolangma Natural Nature Preserve, Tibetan Plateau, and evidence oftransboundary pollutant invasion, Atmospheric Chemistry and Physics, 19, 1373-1391, 10.5194/acp-19-1373-2019, 2019.

Lindberg, S., Bullock, R., Ebinghaus, R., Engstrom, D., Feng, X., Fitzgerald, W., Pirrone, N., Prestbo, E., Seigneur, C., and Panel on Source Attribution of Atmospheric, M.: A synthesis of progress and uncertainties in attributing the sources of mercury in deposition, Ambio, 36, 19-32, 10.1579/0044-7447(2007)36[19:asopau]2.0.co;2, 2007.

Lindberg, S. E. and Stratton, W. J.: Atmospheric Mercury Speciation: Concentrations and Behavior of Reactive Gaseous Mercury in Ambient Air, Environmental Science & Technology, 32, 49-57, 10.1021/es970546u, 1998.

Liu, B., Keeler, G. J., Dvonch, J. T., Barres, J. A., Lynam, M. M., Marsik, F. J., and Morgan, J. T.: Temporal variability of mercury speciation in urban air, Atmospheric Environment, 41, 1911-1923, 10.1016/j.atmosenv.2006.10.063, 2007.

Liu, N., Qiu, G., Landis, M. S., Feng, X., Fu, X., and Shang, L.: Atmospheric mercury species measured in Guiyang, Guizhou province, southwest China, Atmospheric Research, 100, 93-102, 10.1016/j.atmosres.2011.01.002, 2011.

Liu, S., Nadim, F., Perkins, C., Carley, R. J., Hoag, G. E., Lin, Y., and Chen, L.: Atmospheric mercury monitoring survey in Beijing, China, Chemosphere, 48, 97-107, 10.1016/s0045-6535(02)00026-7, 2002.

692   Lynam, M. M., Dvonch, J. T., Hall, N. L., Morishita, M., and Barres, J. A.: Spatial patterns in wet and
693   dry deposition of atmospheric mercury and trace elements in central Illinois, USA, Environmental
694   science and pollution research international, 21, 4032-4043, 10.1007/s11356-013-2011-4, 2014.
695   Pant, N., Ravindra, R., Srivastava, D., and Thompson, L.: The Himalayan cryosphere: past and
696   present variability of the 'third pole', Geological Society, London, Special Publications, 462, SP462.
697   413, 10.1144/SP462.13, 2018.
698   Pokhrel, B., Gong, P., Wang, X., Gao, S., Wang, C., and Yao, T.: Sources and environmental
699   processes of polycyclic aromatic hydrocarbons and mercury along a southern slope of the Central
700   Himalayas, Nepal, Environmental science and pollution research international, 23, 13843-13852,
701   10.1007/s11356-016-6443-5, 2016.
702   Qiu, J.: China: The third pole, Nature, 454, 393-396, 10.1038/454393a, 2008.
703   Rhode, D., Madsen, D. B., Brantingham, P. J., and Dargye, T.: Yaks, yak dung, and prehistoric human
704   habitation of the Tibetan Plateau, Developments in Quaternary Sciences, 9, 205-224,
705   10.1016/S1571-0866(07)09013-6, 2007.
706   Rutter, A. P. and Schauer, J. J.: The impact of aerosol composition on the particle to gas partitioning
707   of reactive mercury, Environ Sci Technol, 41, 3934-3939, 10.1021/es062439i, 2007.
708   Rutter, A. P., Schauer, J. J., Lough, G. C., Snyder, D. C., Kolb, C. J., Von Klooster, S., Rudolf, T.,
709   Manolopoulos, H., and Olson, M. L.: A comparison of speciated atmospheric mercury at an urban
710   center and an upwind rural location, Journal of environmental monitoring : JEM, 10, 102-108,
711   10.1039/b710247j, 2008.
712   Seigneur, C., Vijayaraghavan, K., and Lohman, K.: Atmospheric mercury chemistry: Sensitivity of
713   global model simulations to chemical reactions, Journal of Geophysical Research, 111,
714   10.1029/2005jd006780, 2006.
715   Selin, N. E.: Global Biogeochemical Cycling of Mercury: A Review, Annual Review of Environment
716   and Resources, 34, 43-63, 10.1146/annurev.environ.051308.084314, 2009.
717   Slemr, F., Angot, H., Dommergue, A., Magand, O., Barret, M., Weigelt, A., Ebinghaus, R., Brunke, E.
718   G., Pfaffhuber, K. A., Edwards, G., Howard, D., Powell, J., Keywood, M., and Wang, F.: Comparison
719   of mercury concentrations measured at several sites in the Southern Hemisphere, Atmospheric
720   Chemistry and Physics, 15, 3125-3133, 10.5194/acp-15-3125-2015, 2015.
721   Song, S., Angot, H., Selin, N. E., Gallée, H., Sprovieri, F., Pirrone, N., Helmig, D., Savarino, J., Magand,
722   O., and Dommergue, A.: Understanding mercury oxidation and air–snow exchange on the East
723   Antarctic Plateau: a modeling study, Atmospheric Chemistry and Physics, 18, 15825-15840,
724   10.5194/acp-18-15825-2018, 2018.
725   Sprovieri, F., Gratz, L., and Pirrone, N.: Development of a ground-based atmospheric monitoring
726   network for the Global Mercury Observation System (GMOS), E3S Web of Conferences,
727   10.1051/e3sconf/20130117007,
728   Sprovieri, F., Pirrone, N., Bencardino, M., D'Amore, F., Carbone, F., Cinnirella, S., Mannarino, V.,
729   Landis, M., Ebinghaus, R., Weigelt, A., Brunke, E. G., Labuschagne, C., Martin, L., Munthe, J.,
730   Wangberg, I., Artaxo, P., Morais, F., de Melo Jorge Barbosa, H., Brito, J., Cairns, W., Barbante, C.,
731   Del Carmen Dieguez, M., Garcia, P. E., Dommergue, A., Angot, H., Magand, O., Skov, H., Horvat,
732   M., Kotnik, J., Read, K. A., Neves, L. M., Gawlik, B. M., Sena, F., Mashyanov, N., Obolkin, V., Wip, D.,
733   Feng, X. B., Zhang, H., Fu, X., Ramachandran, R., Cossa, D., Knoery, J., Maruszczak, N., Nerentorp,
734   M., and Norstrom, C.: Atmospheric mercury concentrations observed at ground-based monitoring
735   sites globally distributed in the framework of the GMOS network, Atmos Chem Phys, 16, 11915-

736 11935, 10.5194/acp-16-11915-2016, 2016.

737 Steffen, A., Douglas, T., Amyot, M., Ariya, P., Aspmo, K., Berg, T., Bottenheim, J., Brooks, S., Cobbett,

738 F., and Dastoor, A.: A synthesis of atmospheric mercury depletion event chemistry in the

739 atmosphere and snow, Atmospheric Chemistry and Physics, 8, 1445-1482, 10.5194/acp-8-1445-

740 2008, 2008.

741 Stein, A., Draxler, R. R., Rolph, G. D., Stunder, B. J., Cohen, M., and Ngan, F.: NOAA's HYSPLIT

742 atmospheric transport and dispersion modeling system, Bulletin of the American Meteorological

743 Society, 96, 2059-2077, 10.1175/BAMS-D-14-00110.1, 2015.

744 Stylo, M., Alvarez, J., Dittkrist, J., and Jiao, H.: Global review of mercury monitoring networks, UNEP,

745 Geneva, 2016.

746 Swartzendruber, P., Jaffe, D., and Finley, B.: Improved fluorescence peak integration in the Tekran

747 2537 for applications with sub-optimal sample loadings, Atmospheric Environment, 43, 3648-

748 3651, 10.1016/j.atmosenv.2009.02.063, 2009.

749 Tibet Bureau of Statistics, T.: Tibet Statistics Yearbook, China Statistics Press, Beijing2020.

750 Travnikov, O., Angot, H., Artaxo, P., Bencardino, M., Bieser, J., D'Amore, F., Dastoor, A., De Simone,

751 F., Diéguez, M. d. C., Dommergue, A., Ebinghaus, R., Feng, X. B., Gencarelli, C. N., Hedgecock, I. M.,

752 Magand, O., Martin, L., Matthias, V., Mashyanov, N., Pirrone, N., Ramachandran, R., Read, K. A.,

753 Ryjkov, A., Selin, N. E., Sena, F., Song, S., Sprovieri, F., Wip, D., Wängberg, I., and Yang, X.: Multi-

754 model study of mercury dispersion in the atmosphere: atmospheric processes and model

755 evaluation, Atmospheric Chemistry and Physics, 17, 5271-5295, 10.5194/acp-17-5271-2017, 2017.

756 UNEP, G. M. A.: Sources, Emissions, Releases and Environmental Transport; UNEP Chemicals

757 Branch: Geneva, Switzerland, 2013, 2013.

758 Venter, A., Beukes, J., Van Zyl, P., Brunke, E.-G., Labuschagne, C., Slemr, F., Ebinghaus, R., and Kock,

759 H.: Statistical exploration of gaseous elemental mercury (GEM) measured at Cape Point from 2007

760 to 2011, Atmospheric Chemistry and Physics, 15, 10271-10280, 10.5194/acp-15-10271-2015,

761 2015.

762 Wang, C., Wang, X., Gong, P., and Yao, T.: Long-term trends of atmospheric organochlorine

763 pollutants and polycyclic aromatic hydrocarbons over the southeastern Tibetan Plateau, The

764 Science of the total environment, 624, 241-249, 10.1016/j.scitotenv.2017.12.140, 2018.

765 Wang, X., Gong, P., Wang, C., Ren, J., and Yao, T.: A review of current knowledge and future

766 prospects regarding persistent organic pollutants over the Tibetan Plateau, The Science of the

767 total environment, 573, 139-154, 10.1016/j.scitotenv.2016.08.107, 2016.

768 Wang, X., Zhang, H., Lin, C. J., Fu, X., Zhang, Y., and Feng, X.: Transboundary transport and

769 deposition of Hg emission from springtime biomass burning in the Indo-China Peninsula, Journal

770 of Geophysical Research: Atmospheres, 120, 9758-9771, 10.1002/2015jd023525, 2015.

771 Xiao, Q., Saikawa, E., Yokelson, R. J., Chen, P., Li, C., and Kang, S.: Indoor air pollution from burning

772 yak dung as a household fuel in Tibet, Atmospheric Environment, 102, 406-412,

773 10.1016/j.atmosenv.2014.11.060, 2015.

774 Yang, J., Kang, S., Ji, Z., and Chen, D.: Modeling the Origin of Anthropogenic Black Carbon and Its

775 Climatic Effect Over the Tibetan Plateau and Surrounding Regions, Journal of Geophysical

776 Research: Atmospheres, 123, 671-692, 10.1002/2017jd027282, 2018.

777 Yang, Y., Chen, H., and Wang, D.: Spatial and temporal distribution of gaseous elemental mercury

778 in Chongqing, China, Environ Monit Assess, 156, 479-489, 10.1007/s10661-008-0499-8, 2009.

779 Yao, T., Thompson, L. G., Mosbrugger, V., Zhang, F., Ma, Y., Luo, T., Xu, B., Yang, X., Joswiak, D. R.,

780 Wang, W., Joswiak, M. E., Devkota, L. P., Tayal, S., Jilani, R., and Fayziev, R.: Third Pole Environment
781 (TPE), Environmental Development, 3, 52-64, 10.1016/j.envdev.2012.04.002, 2012.

782 Yin, X., Kang, S., de Foy, B., Ma, Y., Tong, Y., Zhang, W., Wang, X., Zhang, G., and Zhang, Q.: Multi-
783 year monitoring of atmospheric total gaseous mercury at a remote high-altitude site (Nam Co,
784 4730 m a.s.l.) in the inland Tibetan Plateau region, Atmospheric Chemistry and Physics, 18,
785 10557-10574, 10.5194/acp-18-10557-2018, 2018.

786 Yin, X., Zhou, W., Kang, S., de Foy, B., Yu, Y., Xie, J., Sun, S., Wu, K., and Zhang, Q.: Latest
787 observations of total gaseous mercury in a megacity (Lanzhou) in northwest China, The Science of
788 the total environment, 720, 137494, 10.1016/j.scitotenv.2020.137494, 2020.

789 Zhang, H., Fu, X., Lin, C., Wang, X., and Feng, X.: Observation and analysis of speciated atmospheric
790 mercury in Shangri-La, Tibetan Plateau, China, Atmos. Chem. Phys, 15, 653-665, 10.5194/acp-15-
791 653-2015, 2015a.

792 Zhang, H., Fu, X. W., Lin, C. J., Shang, L. H., Zhang, Y. P., Feng, X. B., and Lin, C.: Monsoon-facilitated
793 characteristics and transport of atmospheric mercury at a high-altitude background site in
794 southwestern China, Atmospheric Chemistry and Physics, 16, 13131-13148, 10.5194/acp-16-
795 13131-2016, 2016.

796 Zhang, L., Wang, S., Wang, L., and Hao, J.: Atmospheric mercury concentration and chemical
797 speciation at a rural site in Beijing, China: implications of mercury emission sources, Atmospheric
798 Chemistry and Physics, 13, 10505-10516, 10.5194/acp-13-10505-2013, 2013.

799 Zhang, R., Wang, H., Qian, Y., Rasch, P. J., Easter, R. C., Ma, P. L., Singh, B., Huang, J., and Fu, Q.:
800 Quantifying sources, transport, deposition, and radiative forcing of black carbon over the
801 Himalayas and Tibetan Plateau, Atmospheric Chemistry and Physics, 15, 6205-6223, 10.5194/acp-
802 15-6205-2015, 2015b.

803 Zhou, H., Hopke, P. K., Zhou, C., and Holsen, T. M.: Ambient mercury source identification at a New
804 York State urban site: Rochester, NY, The Science of the total environment, 650, 1327-1337,
805 10.1016/j.scitotenv.2018.09.040, 2019.

806 Zhu, J., Wang, T., Talbot, R., Mao, H., Hall, C. B., Yang, X., Fu, C., Zhuang, B., Li, S., Han, Y., and
807 Huang, X.: Characteristics of atmospheric Total Gaseous Mercury (TGM) observed in urban Nanjing,
808 China, Atmospheric Chemistry and Physics, 12, 12103-12118, 10.5194/acp-12-12103-2012, 2012.

809 Zhu, J., Xia, X., Che, H., Wang, J., Cong, Z., Zhao, T., Kang, S., Zhang, X., Yu, X., Zhang, Y. J. A. C.,
810 and Physics: Spatiotemporal variation of aerosol and potential long-range transport impact over
811 the Tibetan Plateau, China, 19, 14637-14656, 10.5194/acp-19-14637-2019, 2019.

812